Supporting Information

Mechanical Force Provoking Oxygen Vacancies and Pyrolysis Gas Reduction Activity for the Efficient Valorization of Waste Biomass and Li-ion Batteries

Fengyin Zhou[1], Beilei Zhang[2], Hongya Wang[1], Danfeng Wang[1], Xin Qu[1], Shiyu Wang[1], Mengyi Tang[1], Ling Peng[1], Xiang Chen[1], Dihua Wang[1,3,4], Lawrence Yoon Suk Lee[5], Huayi Yin[1,3,4] *

1. School of Resource and Environmental Science, Wuhan University, 299 Bayi Road, Wuchang District, Wuhan 430072, P. R. China.
2. School of Materials Science and Engineering, Henan Normal University, Xinxiang, 453007, P. R. China
3. Hubei International Scientific and Technological Cooperation Base of Sustainable Resources and Energy, Wuhan 430072, P. R. China.
4. Hubei Provincial Key Laboratory of Biomass Resource Chemistry and Environmental Biotechnology, Wuhan 430072, P. R. China.
5. Department of Applied Biology and Chemical Technology and the State Key Laboratory of Chemical Biology and Drug Discovery, The Hong Kong Polytechnic University, Hung Hom, Kowloon, Hong Kong SAR, China.

*Corresponding author. Email: yinhuayi@whu.edu.cn (Huayi Yin)

Number of pages: 50

Text S1 Characterization Methods

The chemical state of the elements on the surface of the solid samples was analyzed using X-ray photoelectron spectroscopy (XPS) with a Thermo Scientific K-Alpha spectrometer (USA). To assess the presence of oxygen vacancies, electron paramagnetic resonance spectroscopy (EPR) was employed, utilizing a Bruker EMXplus-6/1 system (Germany). The phase composition of the samples was determined by X-ray diffraction (XRD), using a Panalytical Aeris instrument, with a scanning range of 2θ from 10° to 90°. The morphology of the samples was examined using a MIRA3 LMH field emission scanning electron microscope, equipped with an Aztec Energy X-Max 20 energy dispersive spectrometer.

The enthalpy changes of the materials during heating were investigated using thermogravimetric analysis and differential scanning calorimetry (TG-DSC) on a Netzsch STA 449 F5 model (Germany). The pyrolysis process was analyzed with a thermogravimetric-gas chromatography-mass spectrometry (TGA-GC-MS) system, comprising a TGA 8000 thermogravimetric analyzer, a Clarus680 gas chromatograph, and an SQ-8T mass spectrometer (PerkinElmer, USA). The system was operated in full scan mode to capture the complete spectrum of each data point during the chromatographic analysis. A 1 μL gas sample was injected into the chromatographic column with helium (99.999%) as the carrier gas at a flow rate of 1.0 mL/min. The temperature program involved holding at 40 °C for 2 minutes, followed by a ramp to 300 °C at a rate of 8 °C/min. The mass selective detector's electron impact (EI) ion source temperature was set at 200 °C, and the mass spectra were analyzed in the range of 0-300 atomic mass units (amu), with chromatographic peaks identified using the NIST-MS library and related literature.

Additionally, the pyrolysis process was examined using a thermogravimetric-infrared (TG-IR) system, consisting of a German Netzsch STA-2500 thermogravimeter and a US Thermo Fisher IS-50 Fourier transform infrared spectrometer (FTIR). This system enabled real-time analysis of the volatile gases produced during pyrolysis, with continuous scanning mode ensuring that the complete infrared spectrum was captured at each time point. Nitrogen (99.999%) was used as the carrier gas at a flow rate of 50 mL/min, and the temperature program for thermogravimetric analysis involved heating from room temperature to 600 °C at 10 °C/min. The FTIR system had a detection range of 4000–400 cm^{-1}, with a resolution of 4 cm^{-1} and 32 scans. The thermal decomposition behavior and chemical composition of the volatile products were analyzed by correlating the real-time infrared spectra with the mass change curve from the TGA. Characteristic peaks were identified using a standard infrared spectral library and relevant literature.

The components of the generated gas were analyzed using a gas chromatograph (GC9790II). The lithium concentration in the product was determined using an atomic absorption spectrophotometer (PERSEE-A3) to calculate the recovery rate. Lastly, the contact angle was measured with a German Dataphysics OCA 20 contact angle meter, and the thermodynamic data of the reaction were derived from HSC Chemistry 9.0

software.

Text S2 The chemical reactions during the oxygen-free roasting process

The self-decomposition reaction of $LiCoO_2$:

$$4LiCoO_2 = 2Li_2O + 4CoO + O_2(g)\#(1)$$

Carbothermal reduction reaction:

$$4LiCoO_2 + C = 2Li_2O + 4CoO + CO_2(g)\#(2)$$

$$2LiCoO_2 + C = Li_2O + 2CoO + CO(g)\#(3)$$

Gas thermal reduction reaction:

$$2LiCoO_2 + CO(g) = Li_2O + 2CoO + CO_2(g)\#(4)$$

$$8LiCoO_2 + CH_4(g) = 4Li_2O + 8CoO + CO_2(g) + 2H_2O\#(5)$$

$$2LiCoO_2 + H_2(g) = Li_2O + 2CoO + H_2O\#(6)$$

Spontaneous Li_2CO_3 reaction:

$$Li_2O + CO_2(g) = Li_2CO_3\#(7)$$

Carbothermal reduction to the metal reaction:

$$C + 2CoO = 2Co + CO_2(g)\#(8)$$

$$CO(g) + CoO = Co + CO_2(g)\#(9)$$

Text S3 Life Cycle Assessment

We conducted a life cycle assessment (LCA) of the recycling processes using the EverBatt model[1], a closed-loop battery recycling framework developed by Argonne National Laboratory. This model is designed for techno-economic and life cycle analysis of various recycling methods, including pyrometallurgical, hydrometallurgical, direct regeneration, and mechanochemical-thermochemical (Me-The) processes (Fig. S26). Our analysis focuses on evaluating the total energy consumption and greenhouse gas emissions associated with these four recycling methods, deliberately excluding emissions or energy linked to the use of electric vehicles. Additionally, the costs and benefits of these recycling approaches are modeled to provide a comprehensive overview.

In the pyrometallurgical recycling process (Fig. S27), waste lithium is processed in a smelter where the electrolyte and plastic components are combusted to provide heat. The graphite/carbon and aluminum present in the battery serve as reducing agents, while cobalt, nickel, copper, and iron are converted into alloys. The remaining materials, including aluminum oxide, are discarded as slag. The Co/Cu/Fe matte is further treated, followed by solvent extraction and precipitation, ultimately yielding cobalt and nickel compounds suitable to produce new cathode materials.

In the hydrometallurgical recycling process (Fig. S28), separated used batteries are first crushed, and then undergo low-temperature calcination to remove the binder and electrolyte. Physical separation processes then isolate metals such as aluminum, copper, and steel, as well as plastics. A leaching process, followed by solvent extraction and sometimes precipitation, produces cobalt compounds and potential lithium carbonate, both of which are essential for manufacturing new positive electrode materials.

The direct recycling process (Fig. S29) begins with the flotation of the black mass from retired lithium batteries to separate recyclable materials. The black mass is then purified through filtration to remove impurities effectively. The solids from flotation are filtered, dried, and prepared for the subsequent mixing and calcination steps. These materials undergo high-temperature calcination, which restores the battery materials' properties through regeneration technology. After completing two stages of processing with different routes, high-quality regenerated cathode materials are obtained, which can be used to create new lithium battery electrodes or be applied to other high-value sectors.

It is important to note that the commercial pyrometallurgical, commercial hydrometallurgical, and direct regeneration flowsheets presented here are derived from EverBatt 2023 and are reproduced for the reader's clarity and understanding.

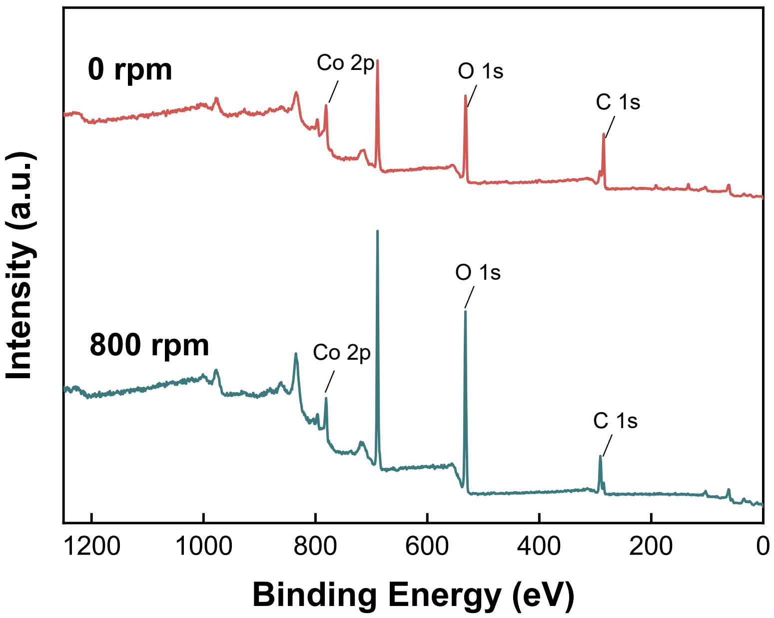

Fig. S1 XPS full spectrum of cathode materials before (0 rpm) and after (800 rpm) mechanical treatment.

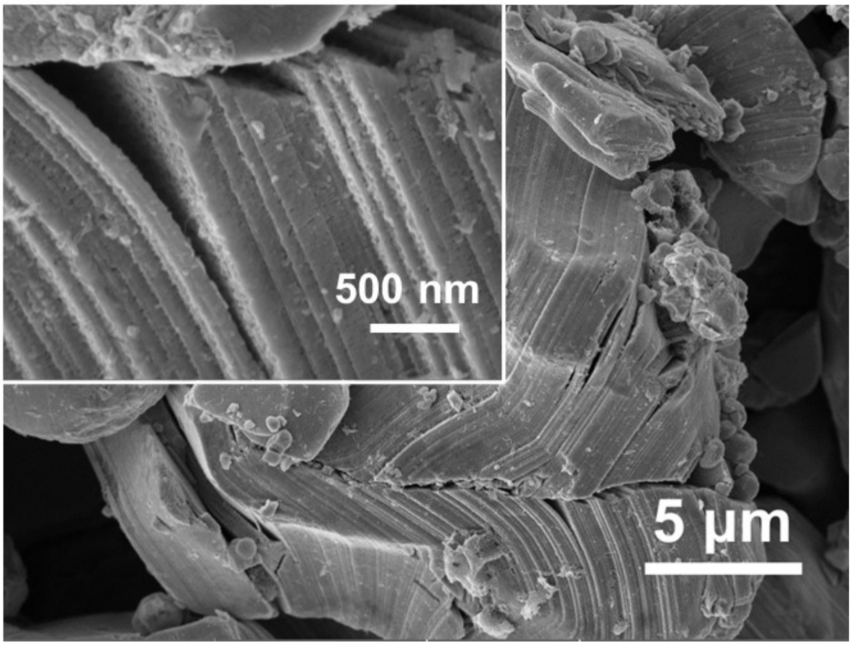

Fig. S2 SEM images of cathode materials before mechanical treatment.

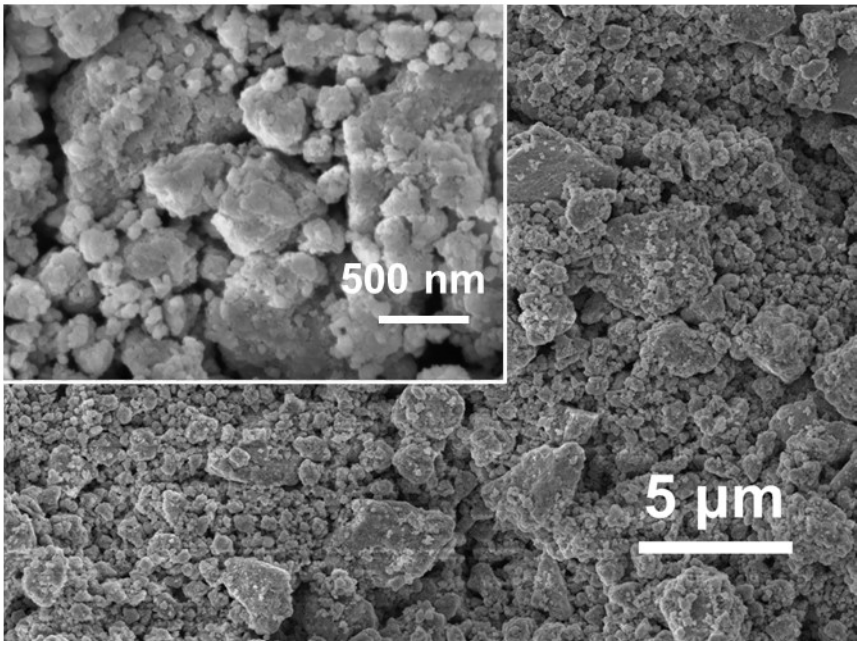

Fig. S3 SEM images of cathode materials after mechanical treatment (800 rpm).

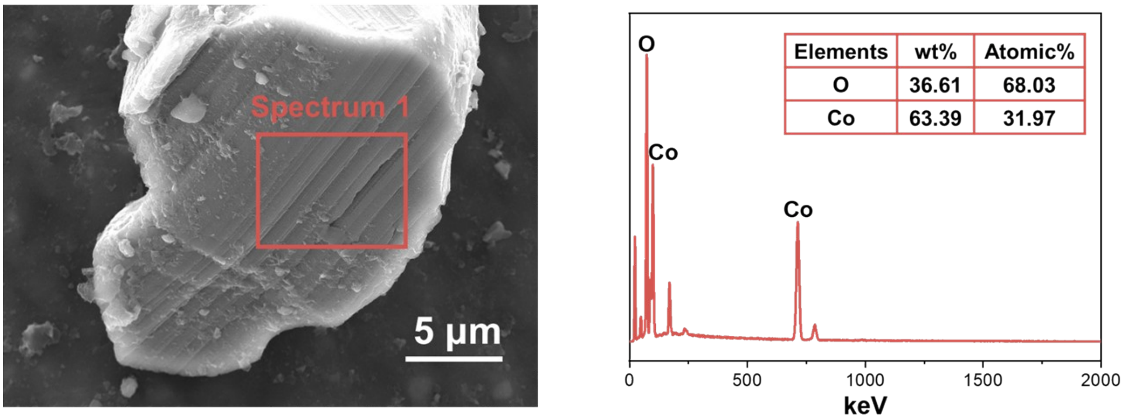

Elements	wt%	Atomic%
O	36.61	68.03
Co	63.39	31.97

Fig. S4 EDS element analysis of cathode materials before mechanical treatment.

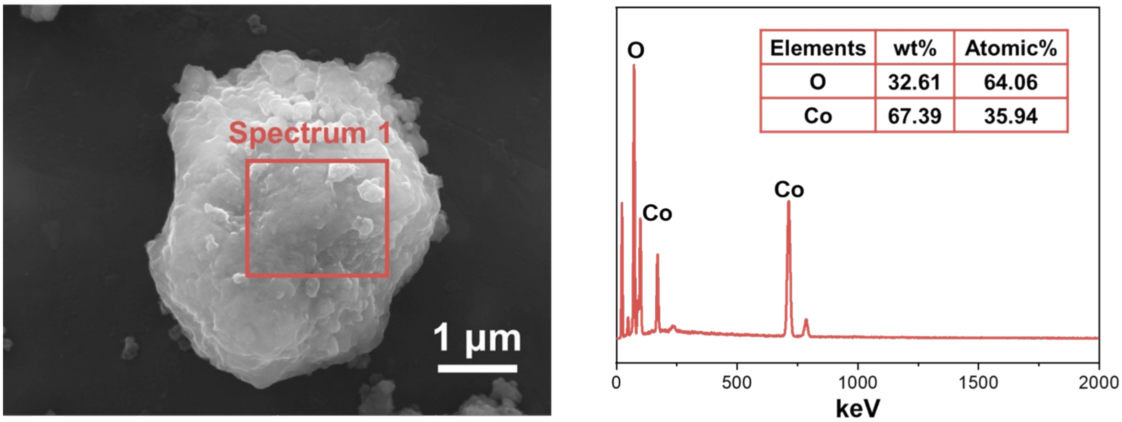

Elements	wt%	Atomic%
O	32.61	64.06
Co	67.39	35.94

Fig. S5 EDS element analysis of cathode materials after mechanical treatment (800 rpm).

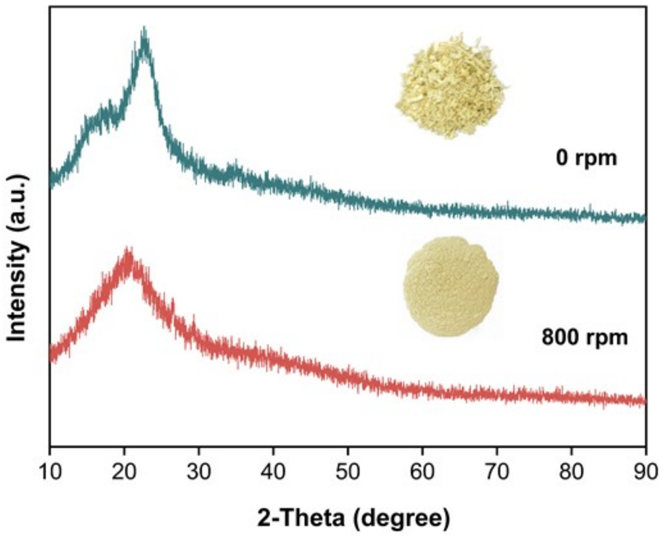

Fig. S6 XRD patterns and digital photos of the sawdust before and after mechanical treatment (800 rpm).

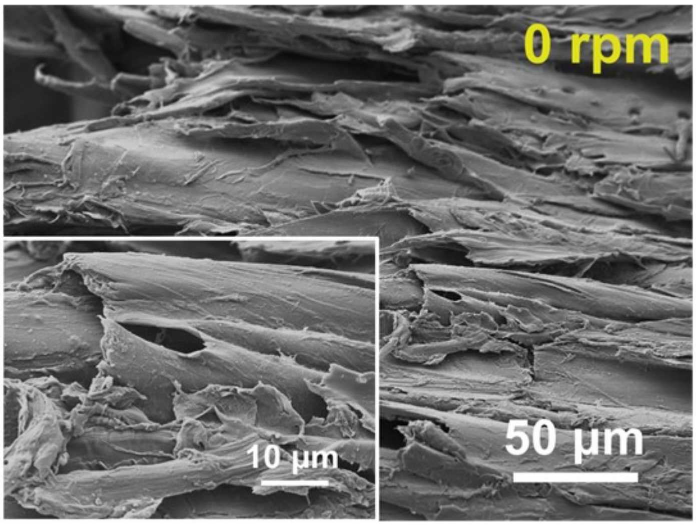

Fig. S7 SEM images of the sawdust before mechanical treatment.

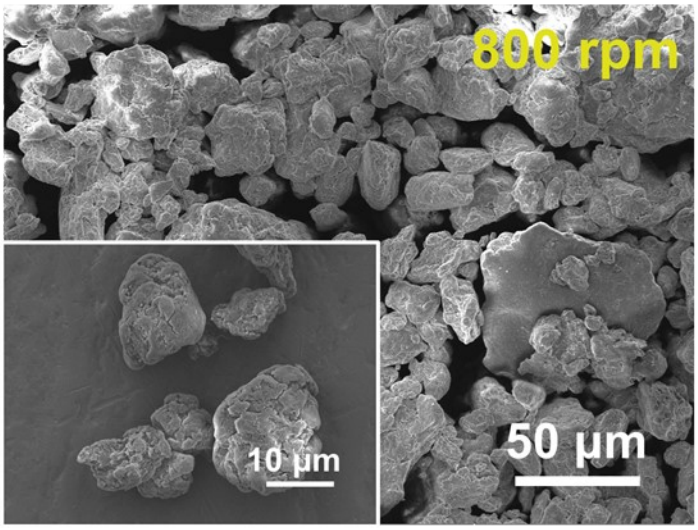

Fig. S8 SEM images of the sawdust after mechanical treatment (800 rpm).

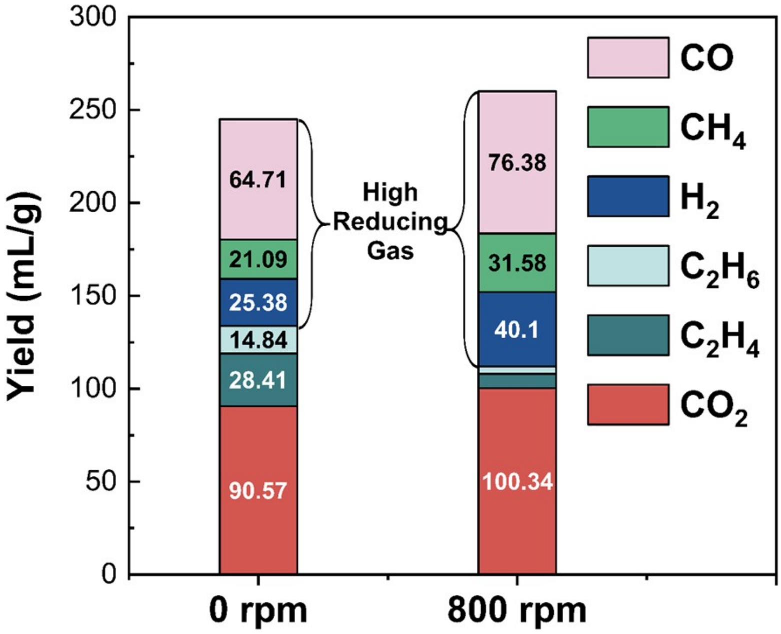

Fig. S9 Gas yield for the sawdust before and after mechanical treatment (800 rpm) while pyrolysis to 800℃.

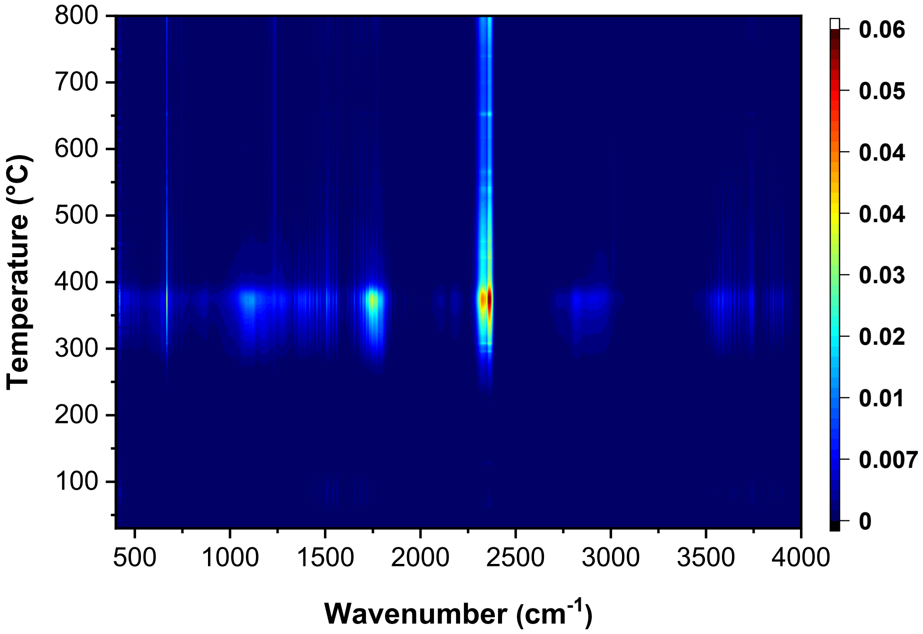

Fig. S10 3D FTIR projection from the pyrolysis of sawdust before mechanical treatment.

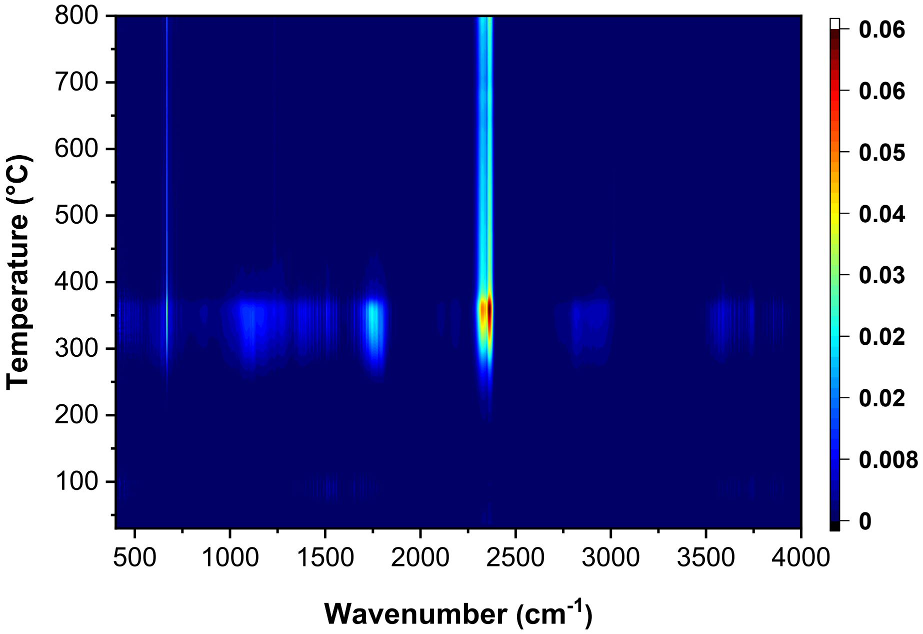

Fig. S11 3D FTIR projection from the pyrolysis of sawdust after mechanical treatment (800 rpm).

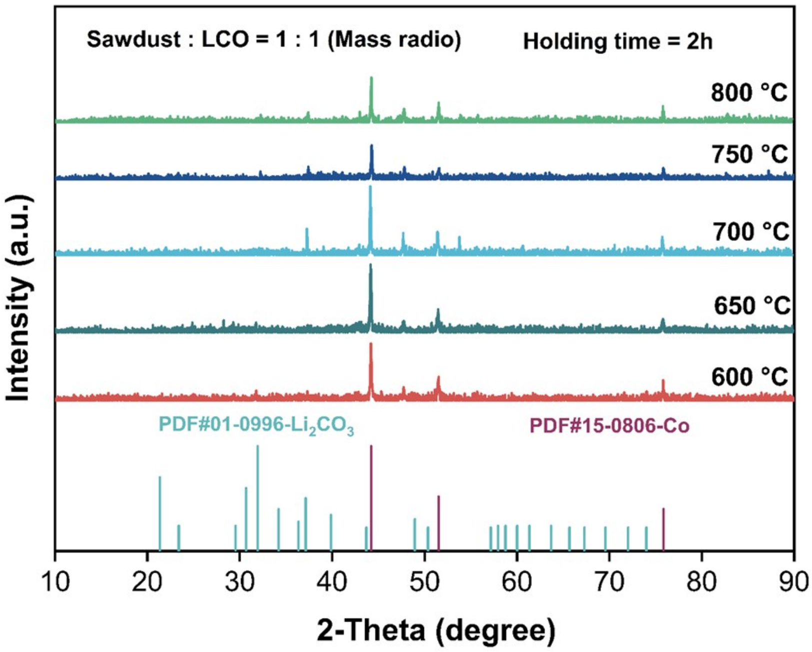

Fig. S12 XRD patterns of the products obtained from oxygen-free roasting of $LiCoO_2$:sawdust =1:1 (mass ratio) for 2h at different temperatures.

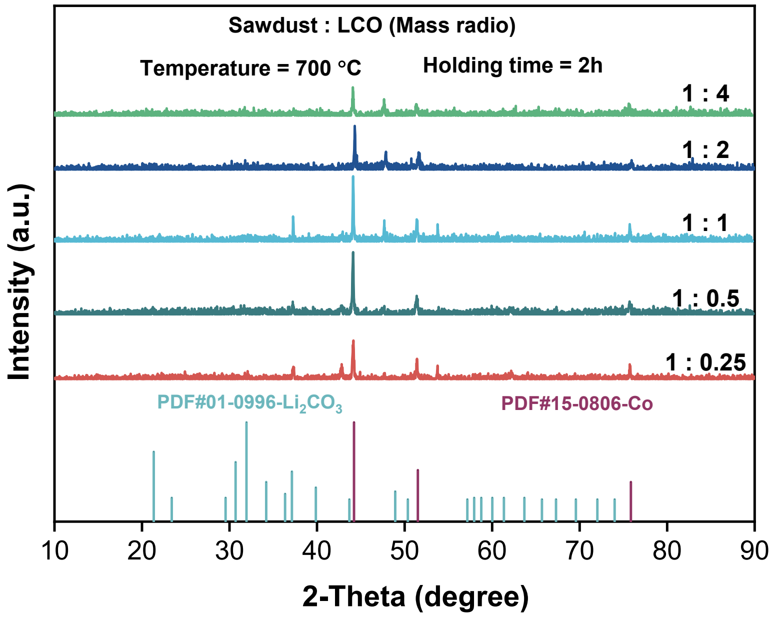

Fig. S13 XRD patterns of the products obtained from oxygen-free roasting of $LiCoO_2$:sawdust performed at 700°C for 2h at different mass ratios.

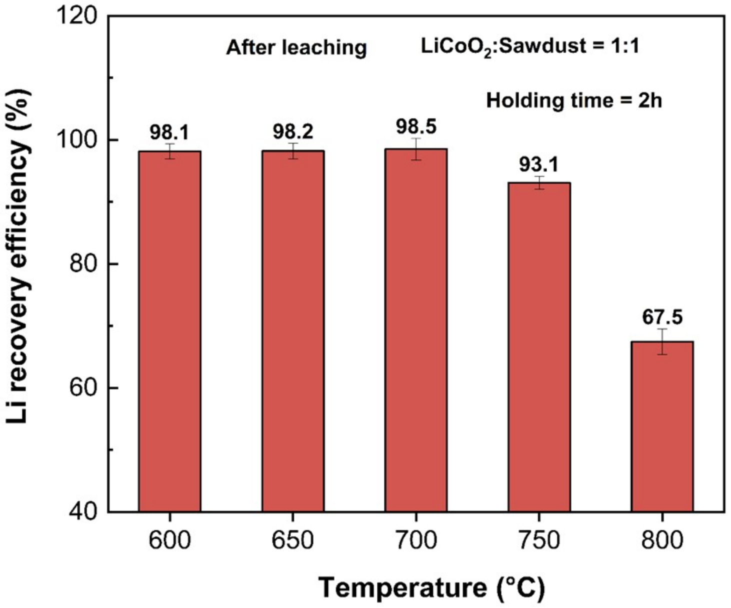

Fig. S14 Li recovery efficiency of the products obtained from oxygen-free roasting of $LiCoO_2$:sawdust =1:1 (mass ratio) for 2h at different temperatures.

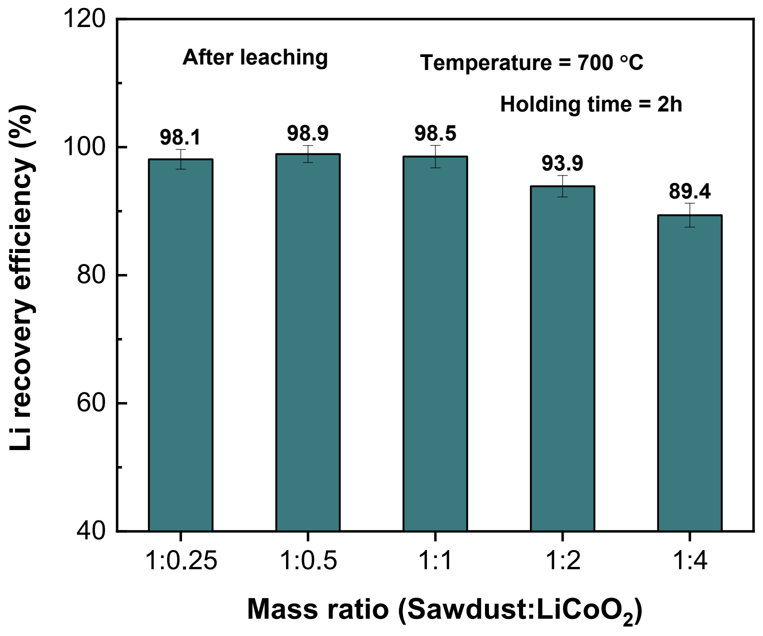

Fig. S15 Li recovery efficiency of the products obtained from oxygen-free roasting of $LiCoO_2$:sawdust performed at 700°C for 2h at different mass ratios.

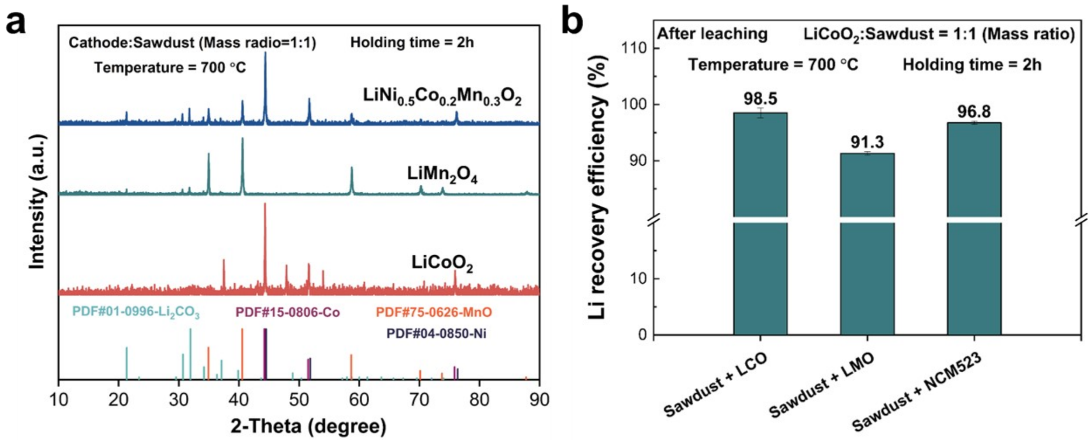

Fig. S16 (a) XRD patterns of the product after ball milling and oxygen-free thermal treatment in different systems, and (b) Li recovery efficiency of the product after ball milling and oxygen-free thermal treatment in different systems.

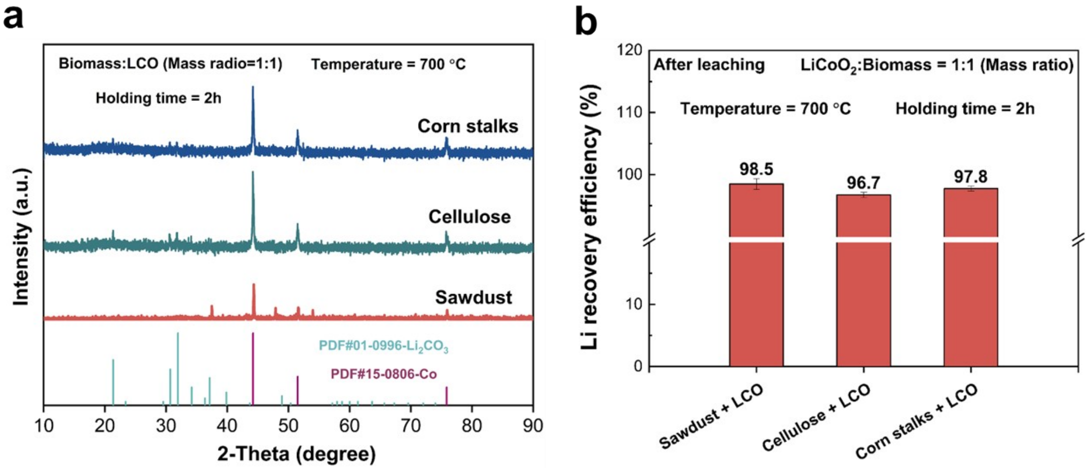

Fig. S17 (a) XRD patterns of the product after ball milling and oxygen-free thermal treatment, and (b) Li recovery efficiency of the product after ball milling and oxygen-free thermal treatment.

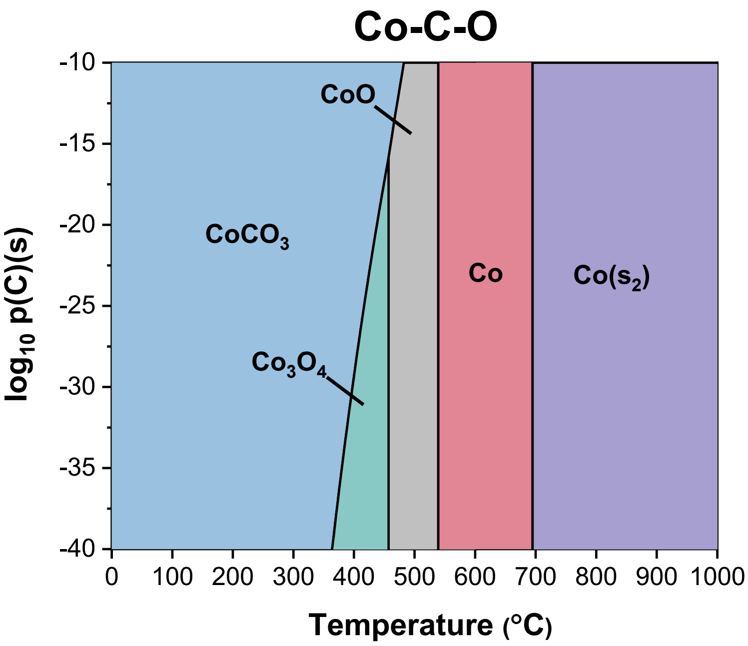

Fig. S18 Predominance diagram for Co-C-O system. (constant value: pO(g) = 1.00 exp (23))

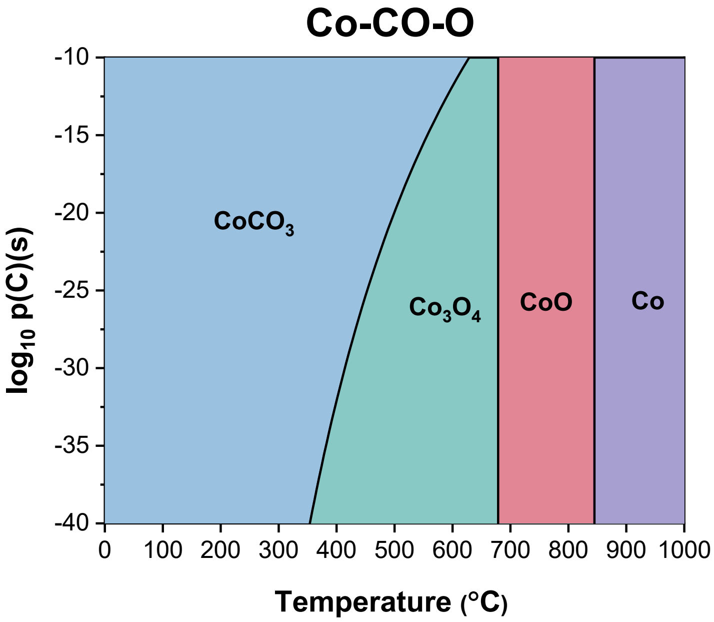

Fig. S19 Predominance diagram for Co-CO-O system. (constant value: pO(g) = 1.00 exp (23))

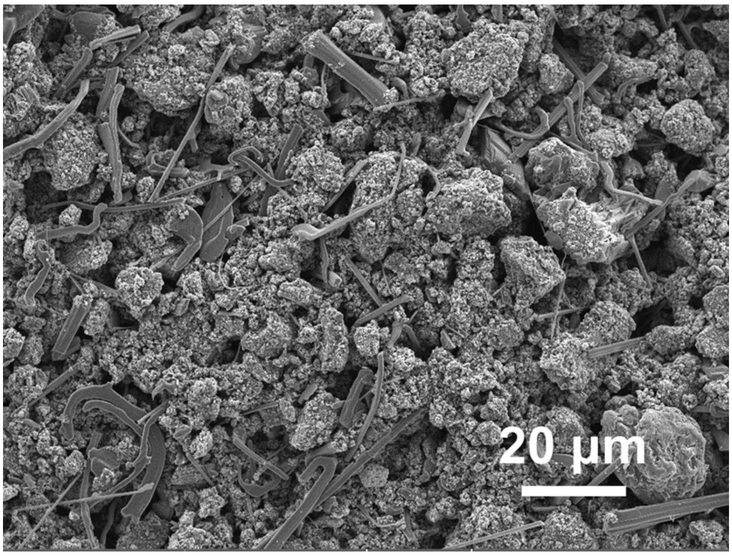

Fig. S20 SEM image of the products obtained from oxygen-free roasting.

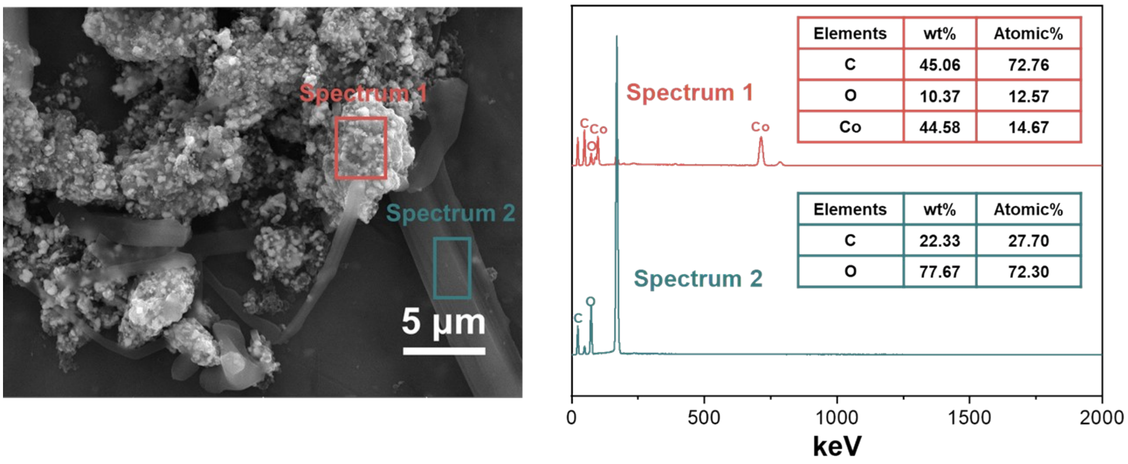

Elements	wt%	Atomic%
C	45.06	72.76
O	10.37	12.57
Co	44.58	14.67

Elements	wt%	Atomic%
C	22.33	27.70
O	77.67	72.30

Fig. S21 EDS element analysis of the products obtained from oxygen-free roasting.

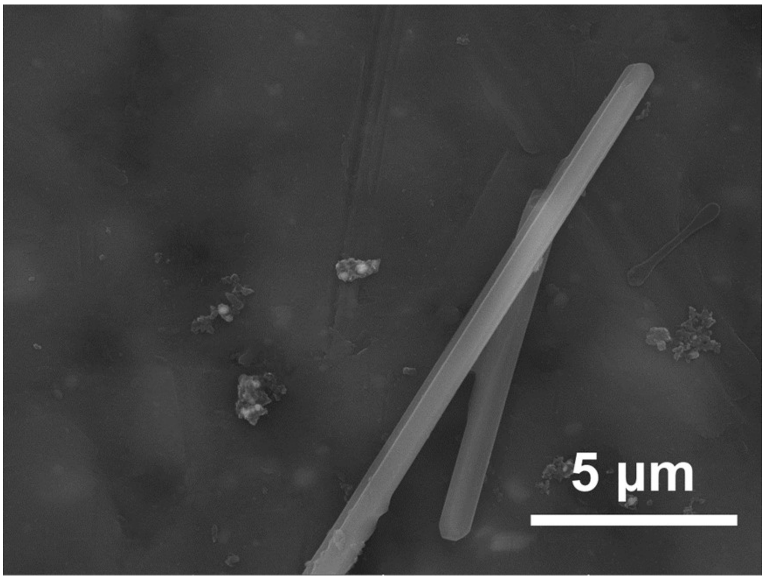

Fig. S22 SEM image of the Li_2CO_3 obtained from water leaching.

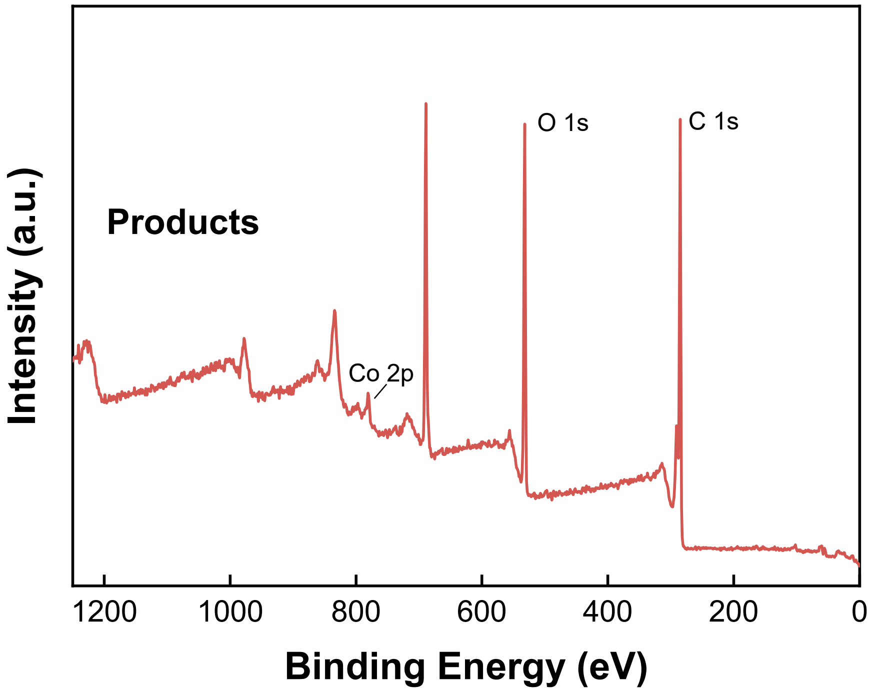

Fig. S23 XPS full spectrum of the products after water leaching separation.

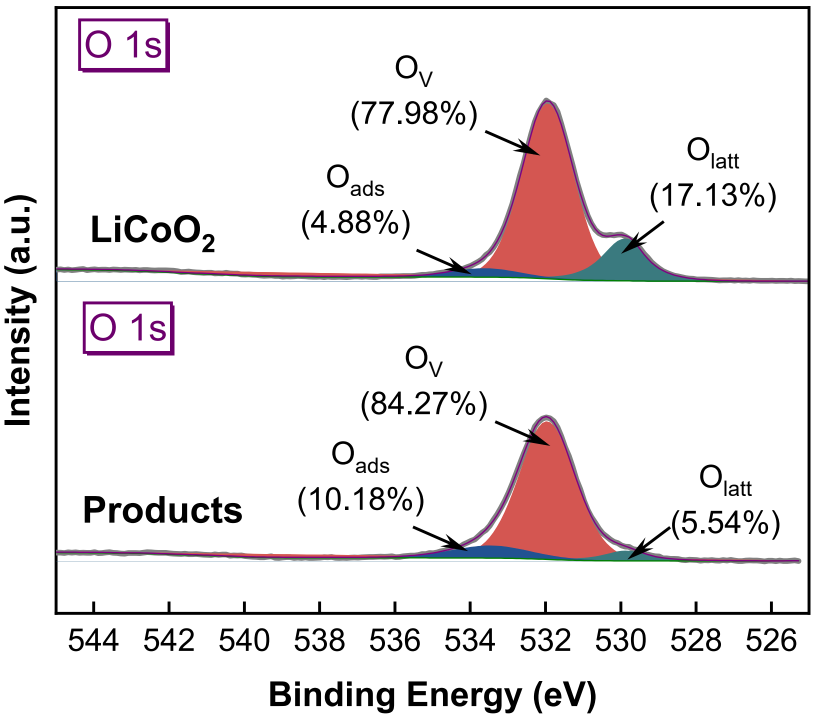

Fig. S24 High-resolution XPS results of O 1s for raw material and products after water leaching separation.

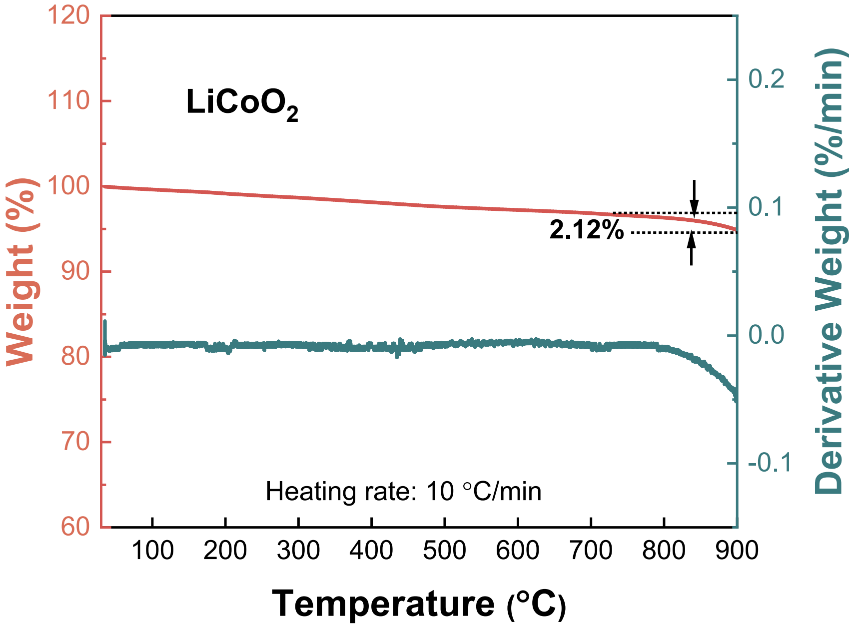

Fig. S25 TG curves of the oxygen-free roasting of LiCoO$_2$.

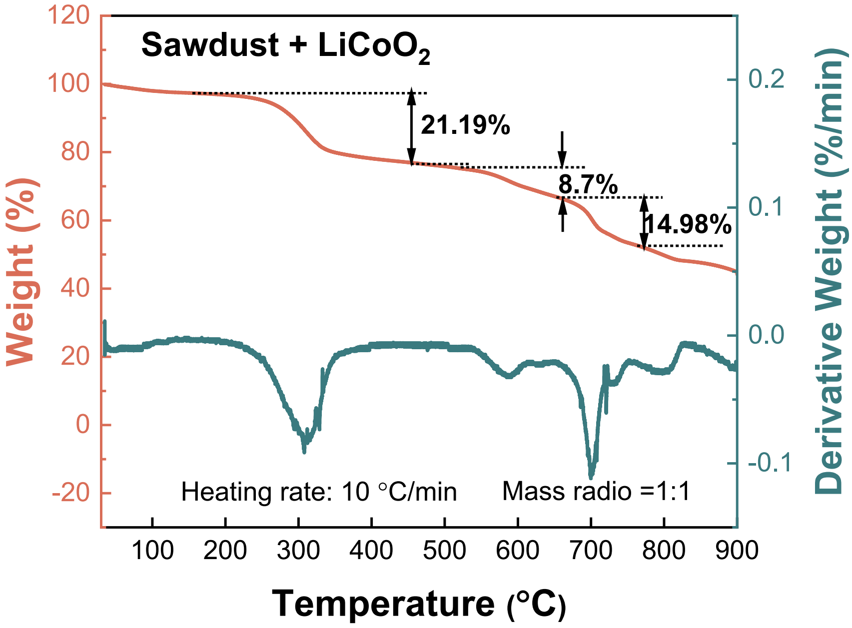

Fig. S26 TG curves of the oxygen-free roasting of $LiCoO_2$:sawdust.(Mass ratio = 1:1)

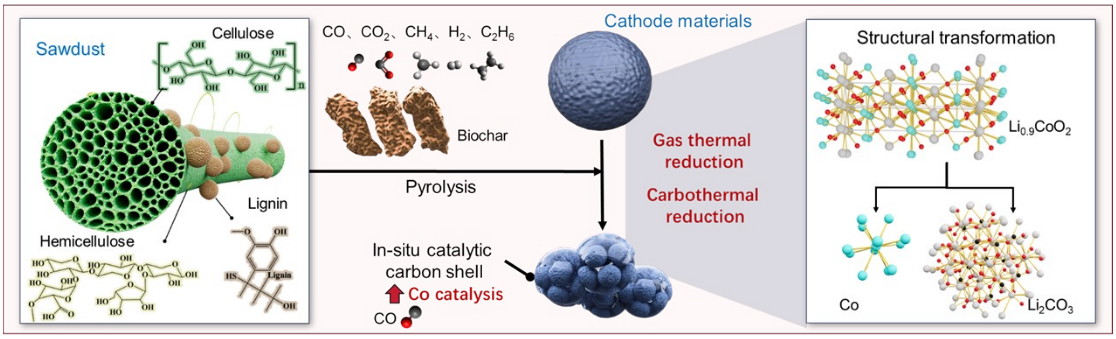

Fig. S27 Schematic diagram of a possible mechanism for the pyrolysis of Sawdust to reduce cathode materials.

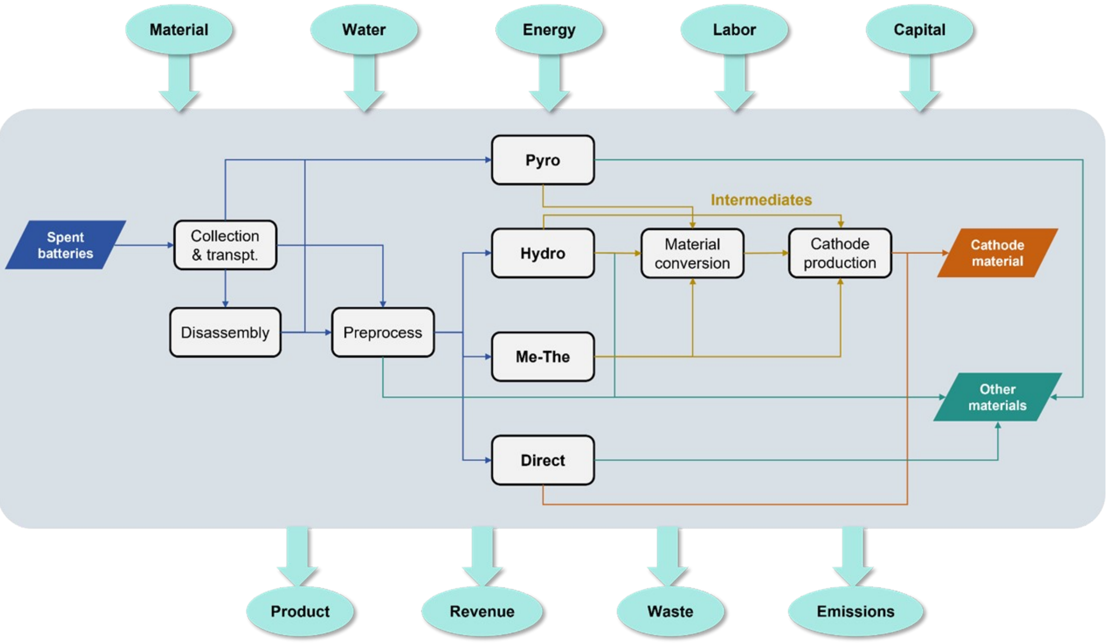

Fig. S28 System Boundary Diagram.

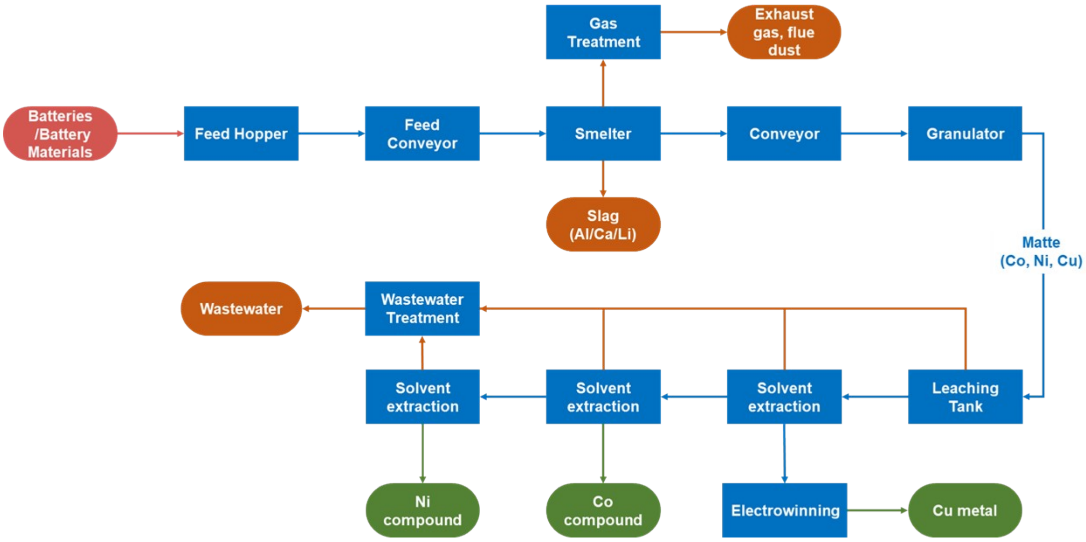

Fig. S29 The pyrometallurgical recycling process.

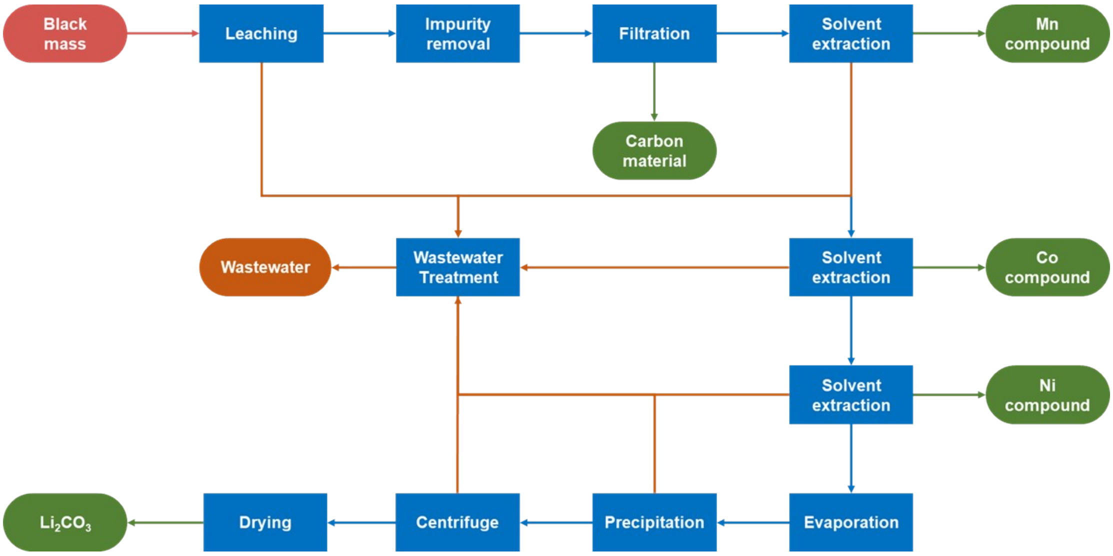

Fig. S30 The hydrometallurgical recycling process.

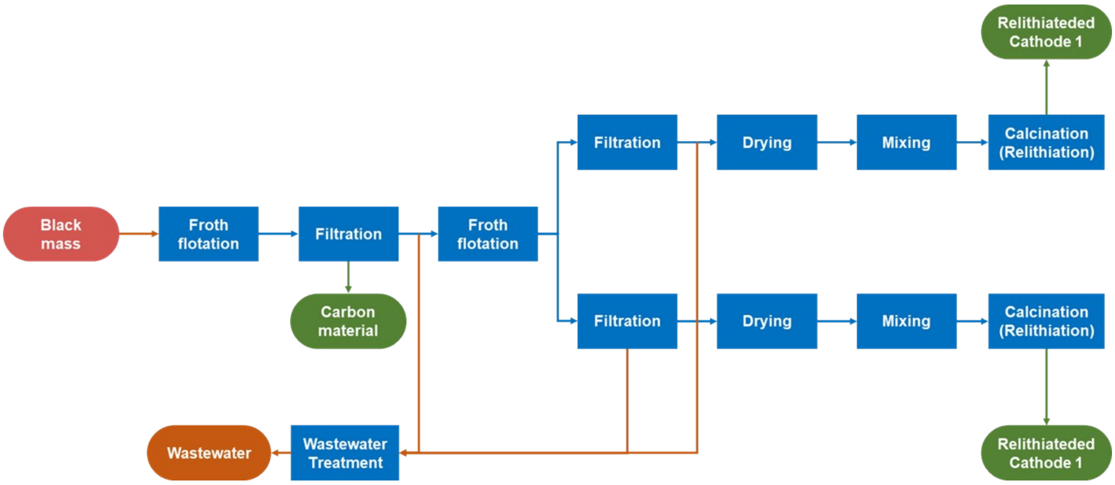

Fig. S31 The direct recycling process.

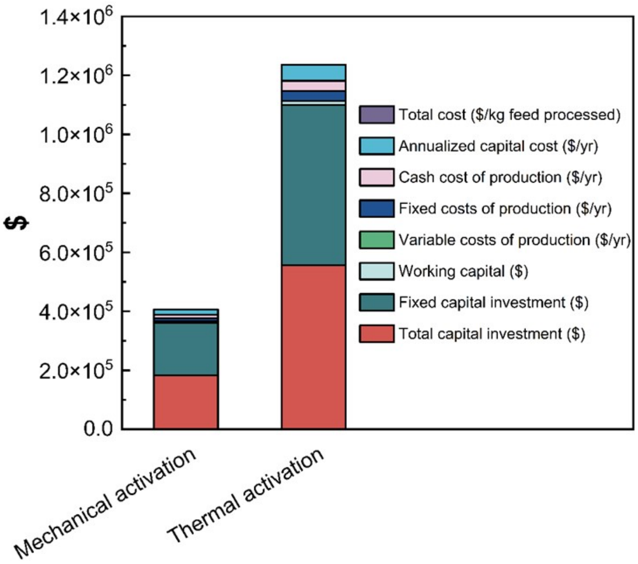

Fig. S32 Cost comparison between mechanical activation (ball milling) and thermal activation (heat treatment furnace)

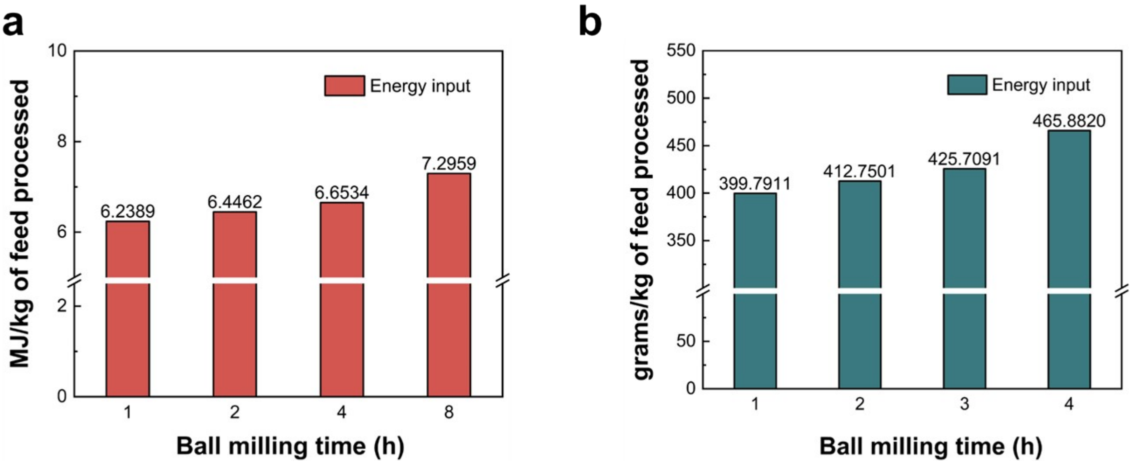

Fig. S33 Sensitivity analysis of different ball milling times: (a) Energy consumption, (b) Greenhouse gas emissions.

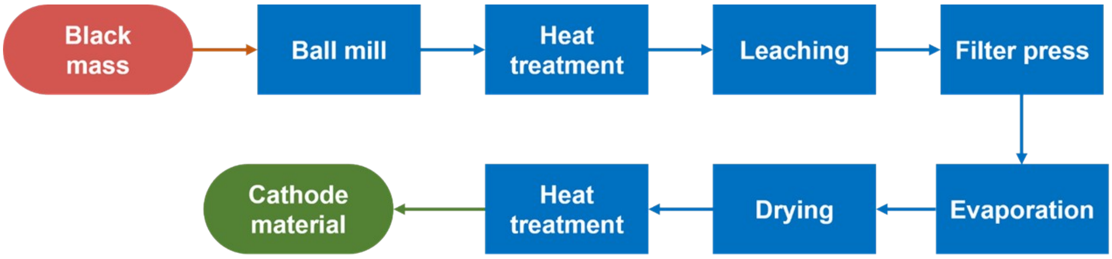

Fig. S34 The mechanochemical-thermochemical process.

Table S1 Rietveld Refinement Results of the cathode material before (0 rpm) mechanical treatment using the EXPGUI software.

Atom	Site	X	Y	Z	Occupancy
	$Li_{0.9}CoO_2$(R_{wp}=8.91%) lattice parameters: *a*=*b*=2.8159 Å, c=13.3976 Å, α=β=90°, γ=120°				
Li	3a	0	0	0.5	1.1847
Co	3b	0	0	0	0.9091
O	3c	0	0	0.2573	0.9671

Atom	X	Y	Z	Occupancy
Co_3O_4 lattice parameters: *a*=*b*=*c*=8.0619 Å, α=β=γ=90°				
Co1	0	0	0	1.0093
Co2	0.625	0.625	0.625	1.0064
O	0.3825	0.3825	0.3825	0.9064

Atom	X	Y	Z	Occupancy
CoO lattice parameters: *a*=*b*=*c*=4.2248 Å, α=β=γ=90°				
Co1	0	0	0	0.9714
O	0.5	0.5	0.5	1.0138

Table S2 Rietveld Refinement Results of the cathode material after (800 rpm) mechanical treatment using the EXPGUI software.

Atom	Site	X	Y	Z	Occupancy
	$Li_{0.9}CoO_2$(R_{wp}=4.99%) lattice parameters: *a*=*b*=2.9320 Å, c=14.2418 Å, α=β=90°, γ=120°				
Li	3a	0	0	0.5	1.4563
Co	3b	0	0	0	0.8998
O	3c	0	0	0.2509	0.9247

Atom	X	Y	Z	Occupancy
Co_3O_4 lattice parameters: *a*=*b*=*c*=8.1051 Å, α=β=γ=90°				
Co1	0	0	0	0.9852
Co2	0.625	0.625	0.625	1.0089
O	0.3898	0.3898	0.3898	1.0402

Table S3 Comparison of $LiCoO_2$ recovery efficiency with literature results.

Reducing agent	Methods	Temperature (°C)	Li recovery efficiency (%)	Ref.
Graphite	Oxygen-free roasting/wet magnetic separation	1000°C	98.93%	[2]
Graphite	Vacuum Metallurgy	700°C	81.90%	[3]
Graphite	Carbothermally-wet magnetic separation	900°C	95.1%	[4]
Graphite	Carbothermic reduction vacuum pyrolysis	700°C	93%	[5]
Graphite+ 10%NaOH	Alkali Metal Salt Catalyzed Carbothermic Reduction	520°C	93%	[6]
Activated carbon	Selective isolation-suspension	700°C	38%	[7]
Macadamia Shells	Microwave Pyrolysis	750°C	93.4%	[8]
Graphite	Dry Grinding - Carbonated Ultrasound-Assisted Water Leaching	600°C	92.25%	[9]
Graphite	Carbothermal reduction	800°C	89%	[10]
Cornstalk	Low-temperature thermochemistry	450°C	94%	[11]
Coal	Cheap carbon thermal reduction	800°C	88.7%	[12]
PVC	Synergetic Pyrolysis	450°C	92.5%	[13]
Sawdust	**Mechanochemical and Thermochemical**	**700°C**	**98.5%**	**This work**

Table S4 Total environmental impacts of recycling.

Recycle				
	Pyro	**Hydro**	**Direct**	**Custom**
Cost per kg feedstock processed	$ 190.83	$ 276.20	$ 263.98	$ 199.35
Energy use in MJ per kg feedstock processed				
Total Energy	3.541	36.844	30.961	14.369
Fossil fuels	4.015	33.589	27.118	13.439
Coal	1.278	10.094	13.738	5.755
Natural gas	1.782	23.656	13.089	3051.816
Petroleum	0.955	5.039	5.491	2.643
Water use in gallon	1.4	4.7	3.1	0.5
Total Emissions in g per kg feedstock processed				
VOC	0.075	0.407	0.362	2.442
CO	0.287	1.708	1.329	0.579
NOx	0.754	3.066	2.926	0.761
PM10	0.062	0.287	0.345	1.783
PM2.5	0.048	0.204	0.242	0.059
SOx	1.519	3.620	1.797	0.100
BC	0.015	0.038	0.043	3.559
OC	0.013	0.056	0.061	0.040
CH4	0.572	5.561	4.112	1817.361
N2O	0.006	0.051	0.038	1819.402
CO2	1,478	2,513	2,270	2,387
CO_2 (w/ C in VOC & CO)	1,478	2,517	2,273	453
GHGs	1,497	2,696	2,406	472
Revenue per kg feedstock processed	$ 15.37	$ 16.52	$ 22.55	$ 24.55

Table S5 Allocation factors.

	Mass			
	Pyrometallurgical	Hydrometallurgical	Direct Physical	Custom
Co2+ in product	77.3%	35.7%		
Lithium carbonate (crude)		20.4%		
LCO			63.6%	69.4%
Graphite		20.4%	23.8%	26.0%
Copper metal	22.7%			
	Economic value			
	Pyrometallurgical	Hydrometallurgical	Direct Physical	Custom
Co2+ in product	95.9%	90.9%		
Lithium carbonate (crude)		8.8%		
LCO			99.9%	99.6%
Graphite		0.2%	0.1%	0.1%
Copper metal	4.1%			

Table S6 Plant information.

Plant information	
	Selected
Hours per day	24
Actual Processing hours per day	20
Days per year	320
Plant life (yr)	10
Plant capacity (tonne per yr)	1,000
Throughput (tonne per year)	100

Table S7. Ball mill equipment details (data source: Everbatt)

Ball mill	
Throughput	27 tonne/yr
Design capacity	768 tonne/yr
Percent of capacity	4%
Electrical Power at design capacity	6.702 kW
Electrical power	0.240 kW
Labor requirements for equipment operation	6 person-hrs/day
Cost of equipment	$39,510

Table S8. Heat treatment furnace equipment details (data source: Everbatt)

Heat treatment furnace	
Throughput	69 tonne/yr
Design capacity	768 tonne/yr
Percent of capacity	9%
Electrical Power at design capacity	5861.111kW
Electrical power	523.827 kW
Labor requirements for equipment operation	12 person-hrs/day
Cost of equipment	$120,208

References

1. Q. Dai, J. Spangenberger, S. Ahmed, L. Gaines, J. Kelly and M. Wang, *EverBatt: A Closed-loop Battery Recycling Cost and Environmental Impacts Model*, Argonne National Laboratory, 2019.
2. J. Li, G. Wang and Z. Xu, *J. Hazard. Mater.*, 2016, **302**, 97-104.
3. J. Xiao, J. Li and Z. Xu, *Environ. Sci. Technol.*, 2017, **51**, 11960-11966.
4. S. Vishvakarma and N. Dhawan, *J. Sustain. Metall.*, 2019, **5**, 204-209.
5. Y. Q. Tang, H. W. Xie, B. L. Zhang, X. Chen, Z. Q. Zhao, J. K. Qu, P. F. Xing and H. Y. Yin, *Waste Manage.*, 2019, **97**, 140-148.
6. W. Wang, Y. Han, T. Zhang, L. Zhang and S. Xu, *ACS Sustain. Chem. Eng.*, 2019, **7**, 16729-16737.
7. S. Maroufi, M. Assefi, R. Khayyam Nekouei and V. Sahajwalla, *Sustainable Mater. Technol*, 2020, **23**, e00139.
8. Y. Zhao, B. Liu, L. Zhang and S. Guo, *J. Hazard. Mater.*, 2020, **396**, 122740.
9. B. Makuza, D. Yu, Z. Huang, Q. Tian and X. Guo, *Resour. Conserv. Recycl.*, 2021, **174**, 105784.
10. X. She, K. Zhu, J. Wang and Q. Xue, *Journal of Chemical Research*, 2022, **46**, 17475198211066533.
11. X. Chen, Y. Wang, S. Li, Y. Jiang, Y. Cao and X. Ma, *Chem. Eng. J.*, 2022, **434**, 134542.
12. Y. Lai, X. Zhu, J. Li, Q. Peng, S. Hu, A. Xia, Y. Huang, Q. Liao and X. Zhu, *Waste Manage.*, 2022, **148**, 12-21.
13. Z. Meng, W. Huang, L. Gao, J. Dai, X. Lu, J. Liu, H. Huang, K. Shih and Y. Tang, *ACS Sustain. Chem. Eng.*, 2022, **10**, 12329-12341.